Appl. Phys. A 77, 229–235 (2003)
DOI: 10.1007/s00339-003-2110-z

Applied Physics A
Materials Science & Processing

F. KORTE
J. SERBIN
J. KOCH
A. EGBERT
C. FALLNICH
A. OSTENDORF
B.N. CHICHKOV✉

Towards nanostructuring with femtosecond laser pulses

Laser Zentrum Hannover e.V., Hollerithallee 8, 30419 Hannover, Germany

Received: 20 November 2002/Accepted: 20 January 2003
Published online: 28 May 2003 •

ABSTRACT Detailed investigations of the possibilities for using femtosecond lasers for the nanostructuring of metal layers and transparent materials are reported. The aim is to develop a simple laser-based technology for fabricating two- and three-dimensional nanostructures with structure sizes on the order of several hundred nanometers. This is required for many applications in photonics, for the fabrication of photonic crystals and microoptical devices, for data storage, displays, etc. Measurements of thermionic electron emission from metal targets, which provide valuable information on the dynamics of femtosecond laser ablation, are discussed. Sub-wavelength microstructuring of metals is performed and the minimum structure size that can be fabricated in transparent materials is identified. Two-photon polymerization of hybrid polymers is demonstrated as a promising femtosecond laser-based nanofabrication technology.

PACS 42.62.-b; 42.65.Re; 52.38.Mf; 82.35.-x

1 Introduction

Rapid progress in the development of ultrafast lasers has opened up new applications and possibilities for high-precision material processing that cannot be realized with traditional laser systems. Femtosecond lasers have established themselves as excellent and universal tools for microstructuring solid materials by direct ablative writing [1–8]. This technique allows large area patterns and high quality microstructures with structure sizes between one and a hundred micrometers to be fabricated. Whereas the ability to microstructure is well established, the ability to nanostructure with femtosecond lasers is still in its infancy. By using tightly focused femtosecond pulses, it is possible to produce sub-micrometer structures. However, it is still unclear how practicable and reliable this technique can be.

At present, the challenge is to develop a simple, reliable and rapid nanofabrication technique. In laser-processing technologies, the minimum achievable structure size is determined by the diffraction limit of the optical system and is on the order of the radiation wavelength. However, this is different for ultrashort laser pulses. By taking advantage of the well-defined ablation (in general, modification) threshold, one can beat the diffraction limit by choosing the peak laser fluence slightly above the threshold value [1]. In this case, only the central part of the beam can modify the material and it becomes possible to produce sub-wavelength structures. Another approach for the production of sub-wavelength structures (which is not discussed here) is to use femtosecond pulses in combination with a scanning near-field optical microscope (SNOM). Applications of this technique for nanostructuring and direct ablative writing have already been demonstrated [9].

In this paper, we report on investigations of possibilities for using femtosecond lasers for nanofabrication with a resolution (structure size) on the order of several hundred nanometers (100–500 nm). First, we present results of recent studies of thermionic electron emission that provide valuable information on the surface electron temperature. Then, we demonstrate sub-wavelength structuring of metals, fabrication of periodic structures in transparent materials, and a two-photon polymerization technique.

2 Thermionic electron emission and surface temperature

For nanostructuring, it is important to concentrate laser energy and to keep it in an extremely small volume during the ablation process. To do this with femtosecond lasers, a better understanding of laser–matter interaction physics and process dynamics (on a femtosecond time scale with a several nanometer spatial resolution) is required. Since the laser pulse energy is first transferred to electrons, their transport and relaxation characteristics are very important for ablation. In this section, electron emission from solid targets irradiated by ultrashort laser pulses is studied. This allows direct information on the instantaneous surface electron temperature to be obtained.

When femtosecond laser radiation is focused onto a solid target, photo- and thermal emission of electrons from the target surface starts promptly. Whereas electron emission due to the photoelectric effect takes place at low electron temperatures, thermionic emission is the dominant mechanism at high electron temperatures. Theoretical estimates [10] and experiments [11] predict that for metals and 100-fs laser pulses, the

✉ Fax: +49-511/2788-100, E-mail: ch@lzh.de

transition from multiphoton to thermionic emission occurs at a laser fluence of 1 mJ/cm^2.

Thermionic electron emission from metals appears when the high-energy tail of the heated electron distribution extends above the vacuum level. In this case, the electron yield J is determined by $J \sim \exp(-W/kT_e^S)$, where W is the work function and T_e^S is the surface electron temperature. Femtosecond heating of metals provides the possibility of transferring laser energy directly into the electron subsystem, leaving the lattice cold. The transient decoupling of the electron and lattice subsystems ($T_e \gg T_l$, where T_l is the lattice temperature) allows very short electron pulses to be generated due to non-equilibrium thermionic emission. Femtosecond electron heating of metals can be described by the following equations:

$$C_e \frac{\partial T_e}{\partial t} = -\frac{\partial Q(z)}{\partial z} - \gamma\,(T_e - T_l) + S\,,$$
$$Q(z) = -\kappa_e \partial T_e/\partial z, \quad S = I_L\,(1-R)\,\alpha \exp(-\alpha z)\,, \qquad (1)$$

where z is the direction perpendicular to the target surface, $Q(z)$ is the heat flux, S is the laser heating source term, I_L is the laser intensity, R and α are the reflectivity and absorption coefficients of the target, C_e is the electron heat capacity (per unit volume), γ is the parameter characterizing the electron–lattice coupling, and κ_e is the electron thermal conductivity.

One can build an approximate solution [7, 12] of (1) in the form of

$$T_e(t,z) = T_e^S(t)\,\frac{1}{\delta - l_e(t)} \times \left[\delta \exp(-z/\delta) - l_e(t)\exp(-z/l_e(t))\right]\,, \qquad (2)$$

where $T_e^S(t)$ is the time-dependent surface electron temperature, $\delta = 1/\alpha$ is the optical penetration depth, and $l_e(t)$ is the electron heat penetration depth. By neglecting the electron–lattice coupling during the laser pulse (which is valid when the laser pulse duration is shorter than the electron relaxation time $\tau_L \ll \tau_e = C_e/\gamma$) and assuming the electron heat capacity is constant (which is valid at sufficiently high electron temperatures), we get for the surface electron temperature at $t \le \tau_L$

$$T_e^S(t) = \frac{1}{\delta + l_e(t)}\,\frac{1}{C_e}\int_0^t (1-R) I_L(\tau) d\tau\,,$$
$$T_e^S(\tau_L) = \frac{1}{\delta + l_e(\tau_L)}\,\frac{(1-R)F_L}{C_e}\,, \qquad (3)$$

where F_L is the laser fluence. These expressions follow directly from the energy conservation law. When $l_e(\tau_L) \gg \delta$ is fulfilled, the surface electron temperature is determined by $T_e^S(\tau_L) \sim F_L/l_e(\tau_L)$.

Usually, the electron heat penetration depth is characterized by a diffusion-like behavior and has a square root dependence on time. However, in the case of a strong electron–lattice non-equilibrium, this can be different. It has been observed that the heat penetration depth in metals irradiated by femtosecond laser pulses can grow linearly with time [13] and can have an even more complicated behavior [14]. The most important consequence of this fact is that when the electron heat penetration depth has a linear dependence on time, at the end of the laser pulse, $l_e(\tau_L) \sim \tau_L$, and the maximum surface electron temperature, $T_e^S(\tau_L)$, is determined by the peak laser intensity $I_L = F_L/\tau_L$.

One should be able to observe this behavior by investigating femtosecond laser-induced thermionic electron emission from metals. The non-equilibrium thermionic emission depends on the surface electron temperature according to $J \sim \exp(-W/kT_e^S)$ and, therefore, can have the following dependence on the peak laser intensity:

$$J \sim \exp(-B/I_L)\,, \qquad (4)$$

where B is a constant. As will be demonstrated below, the thermionic electron emission induced by femtosecond laser pulses does really obey this behavior.

We turn now to a discussion of experimental results. Using femtosecond laser pulses at 780 nm, we investigated the dependence of the thermionic emission on the laser pulse duration for molybdenum targets. In Fig. 1a, the number of photoelectrons generated by a single laser pulse is shown for different pulse durations and energies. As can be seen, the measured electron flux exhibits a dramatic increase for shorter pulse du-

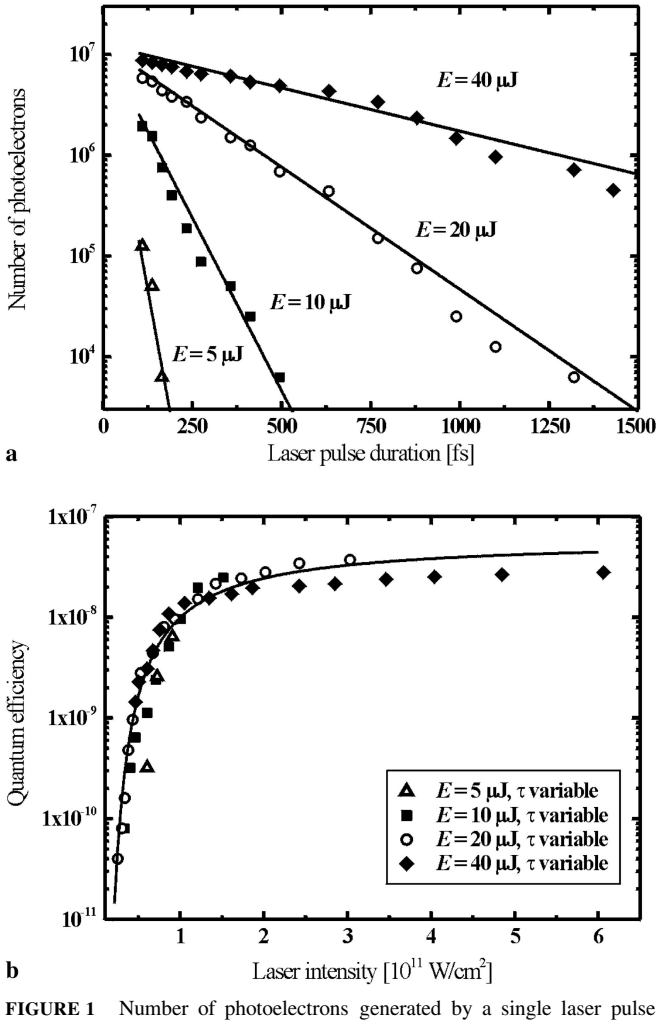

FIGURE 1 Number of photoelectrons generated by a single laser pulse from a molybdenum target as a function of the laser pulse duration **(a)** and dependence of the quantum efficiency on the laser intensity **(b)**. The *solid line* represents a fit according to (4)

rations down to 120 fs. When the quantum efficiency, defined as the number of electrons generated per laser photon, is plotted as a function of laser intensity, we observe that the experimental results shown in Fig. 1a collapse onto a single curve and obey the scaling law given by (4). This is illustrated in Fig. 1b. The solid line represents a fit according to the expression $\eta = 6 \times 10^{-8} \exp(-1.8 \times 10^{11}/I_{\mathrm{L}})$, where I_{L} is the laser intensity in $\mathrm{W/cm^2}$. These results demonstrate, for the first time to our knowledge, that femtosecond thermionic emission is governed by the peak laser intensity. Thus, our assumption of the linear time dependence of the electron heat penetration depth is correct, and the maximum surface electron temperature is really determined by the peak laser intensity. At longer pulse durations (starting from several picoseconds), the photoelectron signal continues to decrease and it seems that the observed dependence changes its character. Detailed investigations of this transition region and further studies of the photoemission properties of other materials are in progress.

The observations reported in this section indicate that, for direct ablative nanostructuring of metals, it is advantageous to use ultrashort laser pulses.

3 Sub-wavelength structuring of metals

In this section, results on the fabrication of sub-wavelength structures in 100–200 nm chromium-coated layers (standard photolithographic masks) are reported. All experiments are performed at atmospheric pressure. To avoid nonlinear aberrations in the microscope objective, the fabrication of sub-micrometer structures is performed with a $36\times / 0.5$ reflective (Schwarzschild) objective.

In Fig. 2, typical scanning-electron microscope (SEM) photographs of surface structures, produced by single laser pulses with different pulse energies, are shown. One can recognize three different processing regimes. In the first low energy regime (Fig. 2a), sub-micron structuring of the chromium layer can be performed. In this regime, the ablation process is usually accompanied by the formation of a small bubble. At higher pulse energies (Fig. 2b), a molten ring around the holes and small droplets can be observed. When the laser pulse energy grows, the size of the hole increases. In the third regime, when the ablation threshold of the glass substrate is reached, sub-micron structuring of the glass substrate becomes possible. The morphology of these structures is typical for transition metals (Cr, Mo, W, Fe) and is determined by the electron–phonon relaxation. For these materials, the transfer of energy to the lattice proceeds much faster than for noble metals [15], which is important for nanostructuring and the fast removal of material.

It is well known that with femtosecond pulses one can overcome the diffraction limit by choosing the peak laser fluence slightly above the ablation threshold (see the schematic illustration in Fig. 3 (left). In this case, only the central part of the beam can ablate the material and it becomes possible to produce sub-diffraction structures. Ablation occurs when $F \geq F_{\mathrm{th}}^{\mathrm{a}}$, which, for a Gaussian beam profile, corresponds to $F = F_0 \exp(-d^2/d_0^2) \geq F_{\mathrm{th}}^{\mathrm{a}}$, where d_0 is the beam diameter. Therefore, for the ablated structure size, one expects the following dependence on the peak laser fluence, $d = d_0[\ln(F_0/F_{\mathrm{th}}^{\mathrm{a}})]^{1/2}$.

To characterize the fabricated structures, we measured the dependence of the hole size on the laser pulse fluence. Experimental data for ablation with 10 pules are shown in Fig. 3 (right). The solid line represents a fit due to $d_0 = 1.250[\ln(F_{\mathrm{th}}^{\mathrm{a}}/0.706)]^{1/2}$ (μm). The minimum reproducible structure size that we were able to fabricate, using 780 nm Ti:sapphire laser radiation focused by the Schwarzschild microscope objective, was 100 nm.

Unfortunately, the fabrication of sub-wavelength holes in metals by tightly focused femtosecond laser pulses is always accompanied by surface modifications (deformations) around the hole. These modifications appear in the area where the applied laser fluence exceeds the melting threshold (see Fig. 3 (left)). One can avoid this effect by using an imaging technique. In Fig. 4, two examples of holes produced by focused laser pulses (left) and by imaging an 80 μm aperture on the

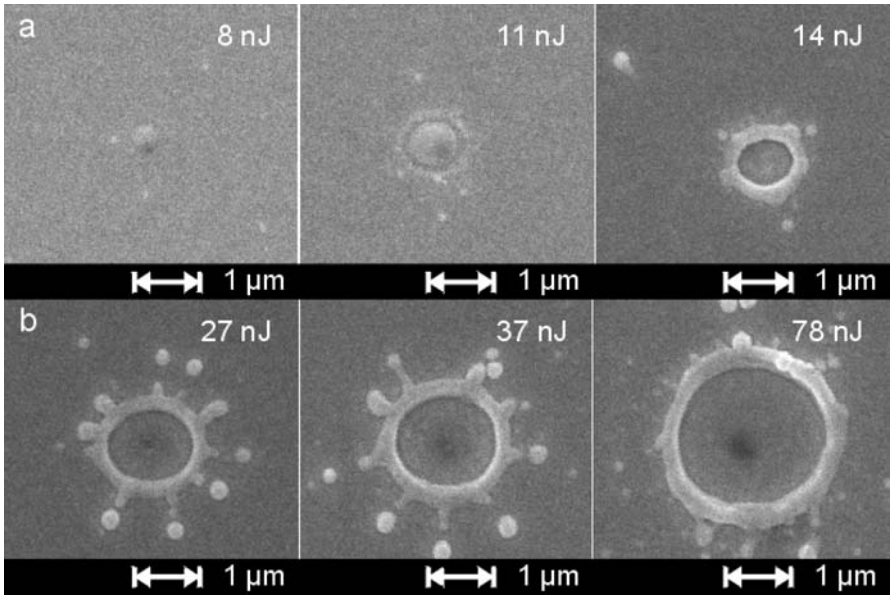

FIGURE 2 Results of the single-pulse laser ablation of a 100 nm chromium

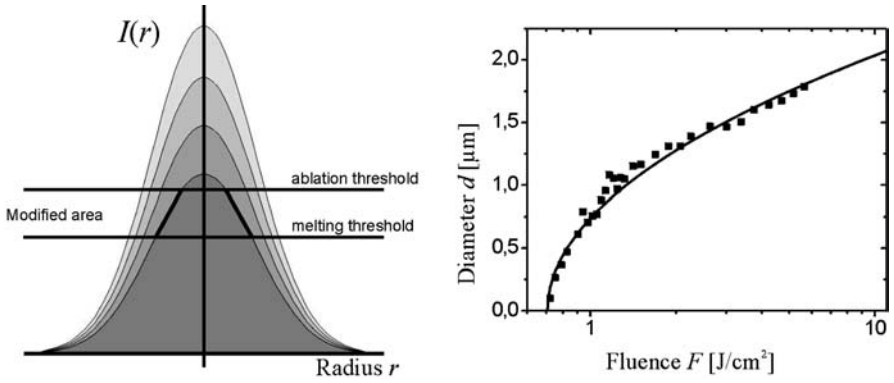

FIGURE 3 Schematic illustration of how one can overcome the diffraction limit by taking advantage of the well-defined ablation threshold (*left*). Dependence of the structure size on the laser pulse fluence for a 100 nm thick chromium target (*right*). The *solid line* represents a fit due to $d_0 = 1.250[\ln(F_{\mathrm{th}}^{\mathrm{a}}/0.706)]^{1/2}$ (µm)

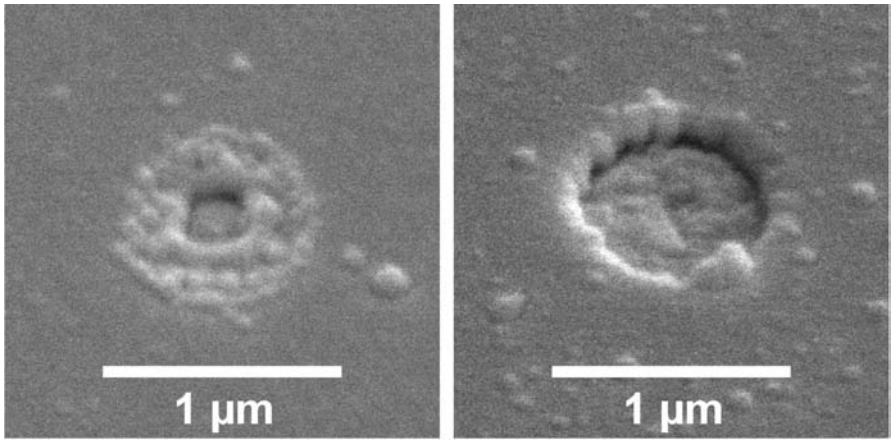

FIGURE 4 Examples of holes produced by two femtosecond laser pulses in a 100 nm chromium layer using focusing (*left*) and imaging (*right*) setup

chromium surface (right) are shown. One can see that the imaging technique allows sub-micrometer holes with very sharp edges to be produced.

4 Nanostructuring of transparent materials

In this section, investigations towards femtosecond laser nanostructuring of transparent materials are reported. Due to the nonlinear nature of the interaction of femtosecond laser pulses with transparent materials, simultaneous absorption of several photons is required to initiate ablation. Multiphoton absorption produces initial free electrons that are further accelerated by the femtosecond laser electric field. These electrons induce avalanche ionization and optical breakdown, and generate a microplasma. The subsequent expansion of the microplasma results in the fabrication of a small structure at the target surface.

To perform nanostructuring, one should carefully control the femtosecond laser intensity distribution in the focus area. This distribution was measured by imaging the corresponding position in the focus onto a CCD camera with a high numerical aperture ($NA = 0.95$) 100× microscope objective. In Fig. 5 (left), the measured laser intensity distribution $I(r)$ in the focus of the Schwarzschild objective is shown. Since the laser interaction process with transparent materials is strongly nonlinear, the actual parameter required for the characterization of ablation is $[I(r)]^q$, where q is the number of photons required to overcome the energy band gap. To illustrate this dependence, the fifth power of the measured laser intensity distribution $[I(r)]^5$ is shown in Fig. 5 (right). It is clear that, due to the nature of nonlinear interaction, one can produce sub-diffraction limited structures. An example of a 200 nm hole fabricated in glass is shown in Fig. 5 (bottom).

The minimum structure size that can be produced by femtosecond laser pulses is determined by the equation $d = k\lambda/NAq^{1/2}$, where λ is the radiation wavelength, NA is the numerical aperture of the focusing optics, and k is a proportionality constant ($k = 0.5$–1). To test this prediction, we investigated the dependence of the minimum structure size that can be fabricated in different transparent materials on their band gap energy. In these experiments, we used a commercial kilohertz femtosecond laser system delivering 1 mJ, 30 fs laser pulses at an 800 nm wavelength, and a 36× Schwarzschild objective with $NA = 0.5$. In measurements of the structure size, an array of 10 holes fabricated with the same laser parameters was always used to obtain better statistics.

The results are shown in Fig. 6 together with the SEM images of typical holes. As can be seen, for transparent materials, the minimum structure size is in good agreement with the above equation. The shape of the fabricated holes is different for different materials. Whereas microstructuring with femtosecond laser pulses has a universal character, results of nanostructuring are material-dependent. In our experiments, we identified a class of materials that are suitable for nanostructuring with femtosecond pulses. An important example is a sapphire crystal, which can be nanostructured with sufficiently high quality. In Fig. 7, a first periodic nanostructure fabricated with femtosecond laser pulses in a sapphire crystal is shown. For each hole, ten laser pulses were used. The total processing time for 216 holes shown in Fig. 7 was 30 s (including the time required for sample positioning). This nanostructure can

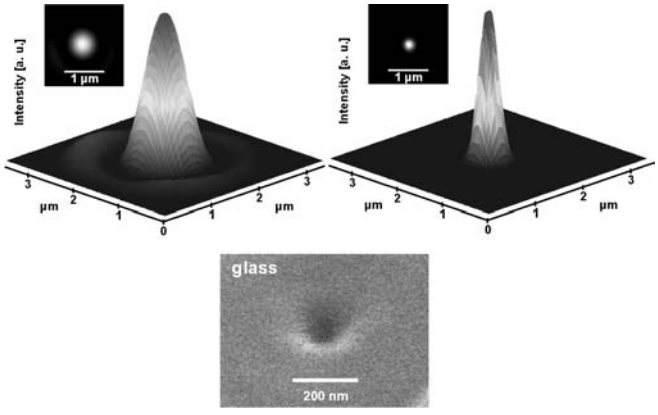

FIGURE 5 Measured laser intensity distribution $I(r)$ in the focus of a Schwarzschild objective (*left*), laser intensity distribution in the fifth power $[I(r)]^5$ (*right*), and an example of a 200 nm hole produced in glass with femtosecond laser pulses (*bottom*)

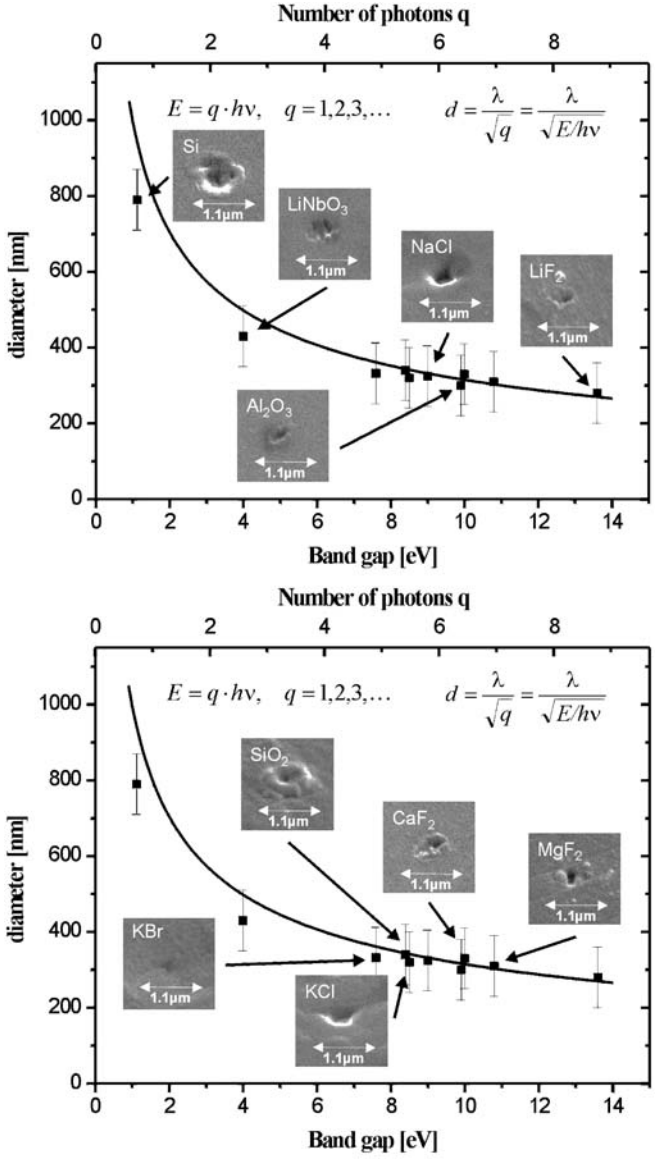

FIGURE 6 Dependence of the minimum structure size for different transparent materials on their band gap energy and SEM images of typical ablation results. The *solid line* represents the structure size calculated due to the expression $d \approx \lambda/q^{1/2}$

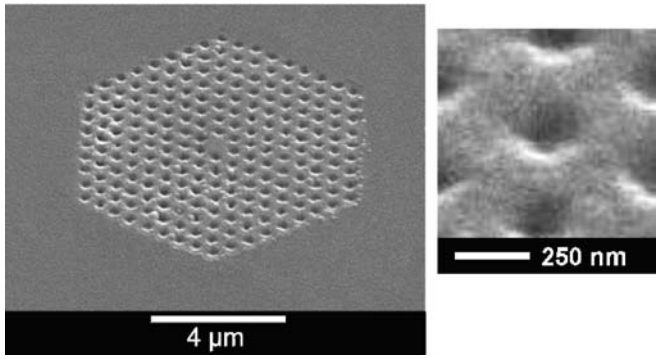

FIGURE 7 An example of a periodic nanostructure (with a defect cavity in the center) fabricated in a sapphire crystal with femtosecond laser pulses (*left*). On the *right side*, an enlarged fragment of a single hole is shown

be considered as a two-dimensional photonic crystal with a defect cavity at the center. Nanostructures analogous to that shown in Fig. 7 are required for many applications in photonics.

5 Two-photon polymerization with femtosecond laser pulses

Another promising possibility for the fabrication of nanostructures is provided by a two-photon polymerization technique. Two-photon polymerization of photosensitive resins, initiated by femtosecond laser pulses, has recently been demonstrated for the fabrication of three-dimensional microstructures [16, 17]. When tightly focused into the volume of a liquid resin that is transparent in the infrared, femtosecond laser pulses can initiate two-photon-polymerization and produce 3D microstructures with a resolution better than 200 nm [17].

In this section, investigations of the two-photon polymerization technique of special hybrid polymers having exceptionally good optical and mechanical properties [18] are reported. The resins we use are designed for ultraviolet photolithography and contain photo-initiators sensitive to 390 nm radiation. These resins are exposed to tightly focused 80 fs Ti:sapphire laser pulses (at 780 nm and a repetition rate of 80 MHz), initiating two-photon polymerization in a small focal volume. Since these resins are transparent to the incident laser light, the polymerization can be initiated everywhere in the volume of the liquid droplet. When the laser focus is moved through the resin in three dimensions, the polymerization occurs along the trace of the focus. This allows the fabrication of any computer-generated 3D structure by direct laser "recording" into the volume of the resin.

In Fig. 8, some examples of 3D microstructures produced by the two-photon polymerization technique are shown. In this figure, SEM images of a 3D periodic structure (top) and a micro-bull statue (bottom) fabricated with femtosecond laser pulses are presented. Corresponding enlarged fragments are shown on the right hand side. Due to the threshold behavior of the two-photon polymerization process, one can fabricate structures below the diffraction limit. In Fig. 9, a SEM image of an array of polymerized voxels (volume pixels), produced on a glass surface using different laser pulse energies and irradiation times (left), is shown. On the right side, an example of a single voxel with a diameter of about

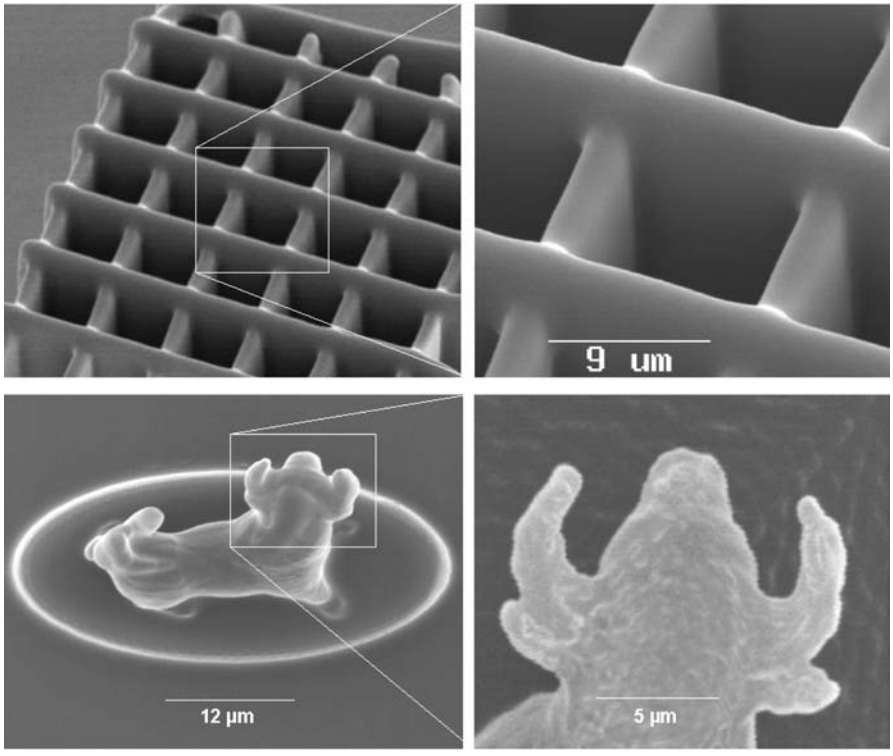

FIGURE 8 SEM images of a three-dimensional periodic structure (*top*) and a micro-bull statue (*bottom*) fabricated by two photon-polymerization in a hybrid polymer using femtosecond laser pulses. Corresponding enlarged fragments are shown on the right side

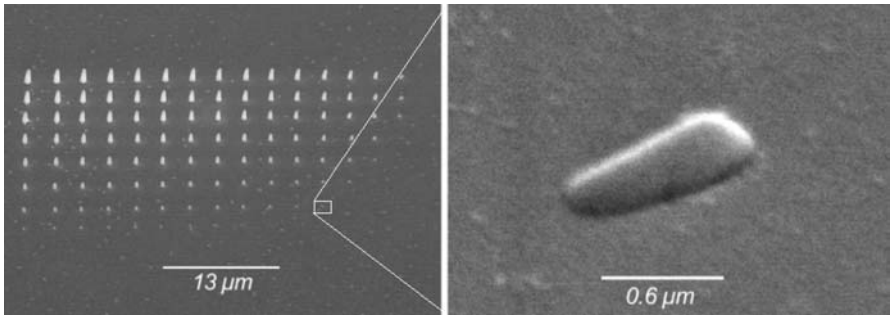

FIGURE 9 SEM images of voxels (volume pixels) produced on a glass surface by two-photon polymeryzation of a photosensitive resin using different laser pulse energies and irradiation times (*left*). Detailed image of a single voxel lying on the surface (*right*)

200 nm and a length of 700 nm, which are determined by the lateral and axial resolution of the focusing objective, is shown. This image represents current resolution limits of our technique. It is expected that, in the future, two-photon polymerization will be used for low-cost fabrication of artificial nanostructured materials for applications in optics, medicine, and biology.

6 Conclusion

High-precision material processing with femtosecond laser pulses has been demonstrated. Femtosecond lasers allow the fabrication of complicated two- and three-dimensional nanostructures with a structure size on the order of several hundred nanometers.

Investigations of thermionic electron emission from metal targets have been performed. These investigations provide valuable information on the dynamics of femtosecond laser ablation. We have observed for the first time that the maximum surface electron temperature in metals irradiated by femtosecond laser pulses is determined by the peak laser intensity. This indicates that for nanostructuring of metals, it is advantageous to use ultrashort laser pulses.

Detailed investigations of nanostructuring of metal layers and transparent materials have been performed. It has been demonstrated that nanostructuring with femtosecond lasers is material-dependent. For different transparent materials, the dependence of the minimum structure size on their energy band gap has been investigated. Using tightly focused 780 nm femtosecond laser pulses, periodic structures with structure sizes down to 200 nm have been fabricated by direct ablative writing at atmospheric pressure.

A high-resolution two-photon polymerization technique of photosensitive hybrid materials has been demonstrated.

REFERENCES

1 P.P. Pronko, S.K. Dutta, J. Squier, J.V. Rudd, D. Du, G. Mourou: Opt. Commun. **114**, 106 (1995)
2 C. Momma, B.N. Chichkov, S. Nolte, F. von Alvensleben, A. Tünnermann, H. Welling: Opt. Commun. **129**, 134 (1996)
3 B.N. Chichkov, C. Momma, S. Nolte, F. von Alvensleben, A. Tünnermann: Appl. Phys. A **63**, 109 (1996)

4 B.C. Stuart, M.D. Feit, S. Herman, A.M. Rubenchik, B.W. Shore, M.D. Perry: J. Opt. Soc. Am. B **13**, 459 (1996)
5 P. Simon, J. Ihlemann: Appl. Phys. A **63**, 505 (1996)
6 W. Kautek, J. Krüger, M. Lenzner, S. Sartania, C. Spielmann, F. Krausz: Appl. Phys. Lett. **69**, 3146 (1996)
7 S. Nolte, C. Momma, H. Jacobs, A. Tünnermann, B.N. Chichkov, B. Wellegehausen, H. Welling: J. Opt. Soc. Am. B **14**, 2716 (1997)
8 See Laser Ablation, Proc. 5th Int. Conf., ed. by J.S. Horwitz, H.-U. Krebs, K. Murakami, M. Stuke. In: Appl. Phys. A **69** (Suppl.), (1999)
9 S. Nolte, B.N. Chichkov, H. Welling, Y. Shani, K. Lieberman, H. Terkel: Opt. Lett. **24**, 914 (1999)
10 S.I. Anisimov, B.L. Kapelovich, T.L. Perel'man: Zh. Eksp. Teor. Fiz. **66**, 776 (1974); Sov. Phys. JETP **39**, 375 (1974)
11 J.G. Fujimoto, J.M. Liu, E.P. Ippen, N. Blombergen: Phys. Rev. Lett. **53**, 1837 (1984)
12 B.S. Luk'yanchuk, S.I. Anisimov, Y.F. Lu: Proc. SPIE **4423** 141 (2001)
13 S.D. Brorson, J.G. Fujimoto, E.P. Ippen: Phys. Rev. Lett. **59**, 1962 (1987)
14 A.P. Kanavin, I.V. Smetanin, V.A. Isakov, Y.V. Afanasiev, B.N. Chichkov, B. Wellegehausen, S. Nolte, C. Momma, A. Tünnermann: Phys. Rev. B **57**, 14 698 (1998)
15 S.-S. Wellershoff, J. Hohlfeld, J. Güdde, E. Matthias: Appl. Phys. A **69** (Suppl.), S99 (1999)
16 B.H. Cumpston, S.P. Ananthavel, S. Barlow, D.L. Dyer, J.E. Ehrlich, L.L. Erskine, A.A. Heikal, S.M. Kuebler, I.-Y.S. Lee, D. McCord-Maughon, J. Qin, H. Röckel, M. Rumi, X.-L. Wu, S.R. Marder, J.W. Perry: Nature **398**, 51 (1999)
17 S. Kawata, H-B. Sun, T. Tanaka, K. Takada: Nature **412**, 697 (2001)
18 J. Serbin, A. Egbert, A. Ostendorf, B.N. Chichkov, R. Houbertz, G. Domann, J. Schulz, C. Cronauer, L. Fröhlich, M. Popall: Opt. Lett. **28**, 301